Evaluating the performance of Lyzenga's water column correction in case-1 coral reef water using a simulated Wolrdview-2 imagery

Masita Dwi Mandini Manessa[1, 2*)], Muhammad Haidar[3], Syarif Budhiman[4], Gatot Winarso[4], Ariyo Kanno[5], Tatsuyuki Sagawa[6], Masahiko Sekine[5]

[1] Graduate School of Science and Engineering, Yamaguchi University, Japan
[2] Center for Remote Sensing and Ocean Science (CReSOS), Udayana University, Denpasar, Bali, Indonesia
[3] Thematic Mapping Division, Geospatial Information Agency of Indonesia
[4] Remote Sensing Application Center, National Institute of Aeronautics and Space (LAPAN)
[5] Graduate School of Sciences and Technology for Innovation, Yamaguchi University, Ube, Japan
[6]Remote Sensing Technology Center of Japan, Tokyo, Japan

*) e-mail: masita@yucivil.onmicrosoft.com, mdm.manessa@gmail.com.

Abstract. This study identified the performance of Lyzenga water column correction under controlled condition of noise, water quality, and bottom type diversity. We build a simulated multispectral imagery, represent the subsurface reflectance of coral reef environment that receives by Worldview-2 satellite. The evaluation was performed to two different subsurface reflectance: Lee et al.'s and Maritonia et al.'s radiative transfer model. As a result, in the case of simple Maritonia et al.'s reflectance model, it shows that the effect of the water column is removable. However, if the actual just above surface reflectance is as more complex as Lee et al.'s model, then the Lyzenga's water column method could reduce the effect of water attenuation but not removed. In fact, based on the mathematical presentation of Lyzenga's model on simulation reflectance formula the effect of depth and water attenuation are in multiplication function. Thus, even after the correction, the water column attenuation effect stillremain.

1. Introduction

The variation of bottom type, water depth, and water attenuation (scattering and absorption in the water column) generated a complicated problem in coral reef mapping. The water attenuation became one of the issues in creating an accurate map. In order to answer this problem Lyzenga[1] proposed an image based correction method to reduce the effect of water attenuation, well known as Lyzenga's water column correction. Since then this correction method has widely applied due to the simplicity. The past publication [2, 3, 4, 5, 6] shows the superiority of this approach with varied accuracy result. Unsurprisingly, many researchers doubt the performance [7, 8]. This opinion built on a fact of Lyzenga's water column correction rely on a lack assumptions; in particular, it assumes no substantial changes in water quality or less diverse bottom types. For the past decade, several studies has

developed a more accurate correction combine the empirical and analytical method such as Purkis [7] and Mishra et al. [8]. However, the availability of optical water parameter used in the analytical method is rare, especially in developing country such as Indonesia. Hence, Lyzenga's method still the best option to be applied in the area with lack water optical data.

As mention before the performance of Lyzenga's water column correction was controlled by the water quality, bottom type diversity, and image noise. A method evaluation using a real imagery was risky because the possibility of error caused by instrument, the time gap of image recording and measurement date, or image noise. Moreover, the actual performance and each parameter effect could not describe precisely. Then this study evaluated the Lyzenga's water column correction under controlled variable, noise, and error. We build a simulated imagery that represents the coral reef environment by combining the measurement and model data.

The usage of simulated imagery to evaluate the performance of water column correction was not for the first time. Zoffoli et al. [9] had performed a similar analysis method to test the performance of an analytical water column correction. Moreover, our simulation set up bears a close resemblance to Zoffoli et al. [9]. However, this study was performed the analysis on the empirical water column correction of Lyzenga [1].

Since there are many radiative transfer model [i.e. 10, 11, 12, 13] to simulated the reflectance received by the satellite. This study used two major models that well known for modelling the reflectance of water surface. First is the simple reflectance model of Maritonia et al. [11] latter be mention as Maritonia et al.'s model. Second is more sophisticated reflectance model of Lee et al. [13] that latter be mention as Lee et al.'s model.

Moreover, our simulation dataset was modeled in hyperspectral range then we convert into the wavelength signature of Worldview-2 Multispectral images as the basis of our study. The Worldview-2 image was intentionally used because it has large visible spectral range than the common multispectral image (SPOT-6, Quickbird, RapidEye, etc.). Especially the coastal band that located in shorter visible wavelength that claims to be useful and sensitive for coastal application such us Coral reef classification mapping or bathymetry.

2. Concept of Lyzenga's Water Column Correction

Lyzenga's proposed the water column correction that based on two assuption: the depth play significant rule in changing the reflectance of object; and water quality is contant all over image. Thus, the radiance or reflectance received by satellite explain that bottom reflectance is exponential relation to water depth and downwelling attenuation. The natural logarithm function of the reflectance value (ρ) was added to linearize the attenuation effect with respect to depth. Thus, a transformed reflectance (X)can be built. In this step of linearization, the Lyzenga method also engages noise correction using the average value of deep-water pixel radiance[9]. The equation of transformed reflectance can be expressed as:

$$X_i = \log(\rho_i - \rho_{\infty i}) \quad (1)$$

Whereρ_i is observed spectral reflectance and$\rho_{\infty i}$represents the water depth-averaged reflectance at band *i*.

Transformed radiance (X) bands i and j are a linear function of water depth (Equation 6) and are linearly relate each other, for a given bottom types (Lyzenga, 1981). Then If the relationship between reflectance and depth is linear and the bottom type is constant, the scatter plot of transformed reflectance (X) bands i and j will fall ideally in a straight line and expressed as:

$$X_i = mX_j + y \quad (2)$$

The slope (m) of this straight line represents the relative attenuation ($\frac{k_i}{k_j}$) in each combination of bands. The different bottom types represented in a scatter plot should create a similar line, the

variation which indicates changes in depth. The gradient of each line would be identical because the ratio of the attenuation coefficients ($\frac{k_i}{k_j}$) is independent of bottom type.

The y-intercept of each line is subsequently used, independent of free of depth, as an index of bottom type; this is known as the depth-invariance index (Yij), which can be written as:

$$Y_{ij} = X_i - \frac{k_i}{k_j} X_j \tag{3}$$

where X_i and X_j represent the transformed radiance at bands i and j, respectively; and ki/kj is the irradiance attenuation coefficient of water in bands i and j. The the ratio of attenuation coefficient (ki/kj) only holds when pixels of the same object at different depths are distributed linearly for the paired bands (Lyzenga, 1978).

3. Simulated Worldview-2 Image

3.1. Overview

Simulated imagery is a simulated the subsurface reflectance based on radiative transfer model for the coral reef environment. The simulated imagery is build base on several assumptions that refer to the condition of the coral reef ecosystem. First, water is very clear and less suspended matter. Second, chlorophyll-α concentration is around 0.02 - 10 mg/m3. Third, clear sky where no significant noises such us cloud, haze, and smokes. Fourth, due to a high spatial imagery then pixel mixing spectral is less. Last, the water surface is calm with no significant white caps.

3.2. Maritonea et al.'s Model

Maritonea et al.'s [11] proposed the surface reflectance function that simplifying assumptions to derive analytical formulae expressing the reflectance of shallow waters as a function of observation depth and bottom depth and albedo. The bottom reflectance assumed as an approximately linear function of the bottom reflectance and an exponential function of the water depth as the same that explain by Lyzenga [1]. Then the just above surface reflectance is written as follows

$$\rho_{rs} = \left(\rho_\infty + \left((p_b - \rho_\infty)e^{-h2K}\right)\right) \tag{4}$$

where ρ_∞ is the in-water volume scattering reflectance at infinite depth, ρ_b is the bottom reflectance, K is the effective attenuation coefficient, and h is water depth. Note that the coefficient $2K$ in Equation (4) is downweliing and upwelling diffuse attenuation coefficient that assumes equal to the vertical diffuse attenuation coefficient for upward flux.

The calculation of K or attenuation coefficient and ρ_∞or reflectance at infinite depth was refer to Morel and Maritonia [11] as follows

$$K(z,\lambda) = K_w(\lambda) + K_{bio}(z,\lambda) \tag{5}$$

$$K_{bio}(z,\lambda) = X(\lambda)(Chl(z))^{e(\lambda)} \tag{6}$$

$$K_w(\lambda) = a_w(\lambda) + (1/2)b_w(\lambda) \tag{7}$$

$$\rho_\infty = \frac{b_b(\lambda,z)}{a_w(\lambda)} \tag{8}$$

$$b_b(\lambda,z) = (1/2)b_w(\lambda) + b_{pb}(\lambda,z) \tag{9}$$

$$b_{pb}(\lambda,z) = \left(0.002 + 0.02\left(0.50 - 0.25\, log_{10}(Chl(z)(550/\lambda))\right)\right) \cdot (0.30(Chl(z)^{0.62}) - b_{w\,550}) \tag{10}$$

where a_w and b_w stand for the absorption and scattering coefficients of optically pure sea water, respectively. a_w , b_w , X and e for each specifiec wavelenght is refer to Table 2 in Morel and Maritonia (2001).

3.3 Lee et al.'s Model

The subsurface reflectance model by Lee et al. [13] was the basis in the Hydrolight Software and had been widely used. The remote sensing the just above surface reflectance for nadir-viewing as follow:

$$\rho_{rs} \approx \frac{0.5 r_{rs}}{1 - 1.5\, r_{rs}} \tag{11}$$

$$r_{rs} = \left(r_{rs}^{dp} \left(1 - e^{-\left[\frac{1}{\cos(\theta_s)} + D_u^C\right] kH} \right) + \frac{\rho_b}{\pi} e^{-\left[\frac{1}{\cos(\theta_s)} + D_u^B\right] kH} \right) \tag{12}$$

with r_{rs}^{dp} is the subsurface reflectivity of the deep water; ρ_b is the bottom reflectance; θ_s is subsurface solar zenith angle; D_u^c and D_u^B are the optical path-elongation factors for scattered photons from the water column and the bottom, respectively; k is the attenuation coefficient; and H is the depth.

The radiative transfer equation parameters depend greatly on the optical properties of the water expressed by

$$r_{rs}^{dp} \approx \left(0.084 + 0.17 u(z,\lambda)\right) u(z,\lambda) \tag{13}$$

$$u(z,\lambda) = \frac{b_b(z,\lambda)}{a(z,\lambda) + b_b(\lambda z,\lambda)} \tag{14}$$

$$k(z,\lambda) = a(z,\lambda) b_b(z,\lambda) \tag{15}$$

$$D_u^c\,(z,\lambda) \approx \sqrt{1.03(1 + 2.4 u(z,\lambda))} \tag{16}$$

$$D_u^b(z,\lambda) \approx \sqrt{1.04(1 + 5.4 u(z,\lambda))} \tag{17}$$

$$b_b(z,\lambda) = b_w(\lambda) + b_{bp}(z,\lambda) \tag{18}$$

$$a(z,\lambda) = a_w(\lambda) + a_p(z,\lambda) + a_y(z,\lambda) \tag{19}$$

with u is the backscattering diffuse attenuation ratio;a_w , a_p, a_y are the attenuation coefficients for pure water, chlorophyll-bearing particles, and covarying yellow matter (CDOM); b_w, b_{bp} are the backscattering coefficient for water and particles. z is chollorophil-a consentration (mg/m3). λ is wavelength (nm).

3.4 Input Parameters

The most abundant bottom types group in shallow coral reef ecosystem are divided as a substrate, life coral, dead coral, and algae. Although these features have different spectral characteristic and can separate as homogenous pixels, in reality, there can be a significant amount of intermixing between these features. This research is focusing on evaluating the homogenous feature and neglected the possibility of various features in each pixel. Moreover, each bottom type was set to have the same distribution of depth and IOP value (Figure 1). Then the inputs value to calculate the just above surface reflectance in equation a and b is shown in Figure 1 and details as follow:

1. TOA solar zenith angle (θ_s) set as 30 then it convert to subsurface solar zenith angle (θs) using Fresnel equation.
2. Depth (H) is 35 random number in normalizing distribution from 0.5 – 19 meter
3. Inherent optical properties (IOP) of D_u^c, D_u^B , V, k, and Kare modeled based on Chlorophyll concentration (z), then we set the Chlorophyll concentration (z) around 0.2 – 0.25 mg m^{-3}

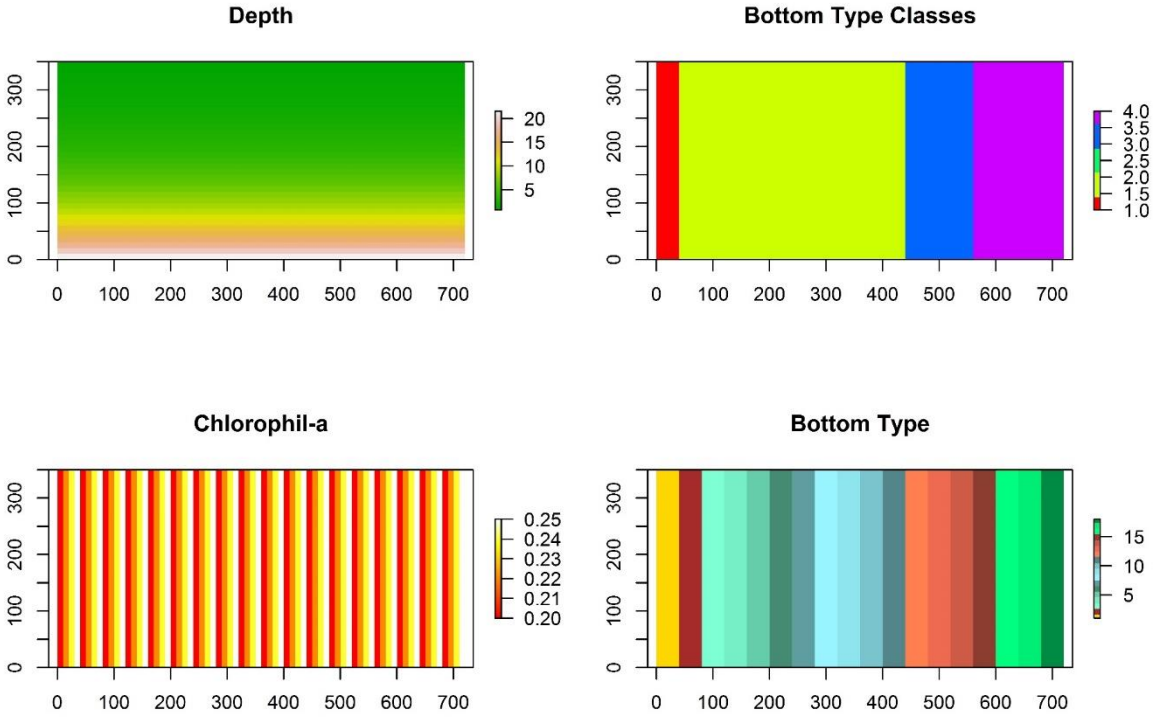

Figure 1. Input data to build the artificial imagery (a) Depth distribution, (b) five bottom type classes (from left to right: class 1: Substrate, class 2: Life coral, class 3: Dead coral, class 4: Algae), (c) Chlorophyll-a distribution, (d) 18 bottom Types distribution (from left to right: Sand, Cyanobacteria, *Acropora sp.*, *Porites sp.*, *Galaxea sp.*, *Heliopora*, *Sinularia sp.*, Coral, Xenia, Softcoral, *Porites sp.*, Dead Coral Tuft Algae, Dead Coral Coralline Algae, Dead Coral Bleaching, Coralline algae)

4. Bottom reflectance (ρ_b) is 18 type of bottom type of one sand, ten coral reefs, four dead corals, and three algae that measured in Derawan (Marlina, 2004)

Furthermore, the full spectral of simulated imagery were converted to each three multispectral bandwidth Rrs (*i.e.*, blue band, green band, and red band) with the following equation [14]:

$$R_{rs}^{wv}(B_i) \approx \frac{\int_{400}^{700} R_{rs}(\lambda) F_{Bi}^{wv}(\lambda) d}{\int_{400}^{700} F_{Bi}^{wv}(\lambda) d} \tag{20}$$

With F_{Bi}^{wv} as the Multispectral bands response function for band i.

3.5 Simulated Image of Coral Reef Environment

Figure 2 shows the simulated image from Maritonia et al.'s model. In the shorter wavelength band (Coastal – Blue bands) some dark bottom type such as algae were unable to model because the object bottom reflectance have smaller reflectance value than deep water ($\rho_\infty > p_b$) and shows as blank white color in Figure 2(a) and 2(b). Based on Maritonia et al.'s based simulated image result, two points can be marked as a note. First, even in the real multispectral image data, all coral reef bottom type can show value, but it not contains a bottom reflectance information. In the case of a dark object, there are opportunities that reflectance received by satellite is just the noise from the water column, water surface, and atmosphere. Second, significant removal of the bottom type in shorter wavelength shows opposite result from the positive claim of Coastal band in Worldview-2.

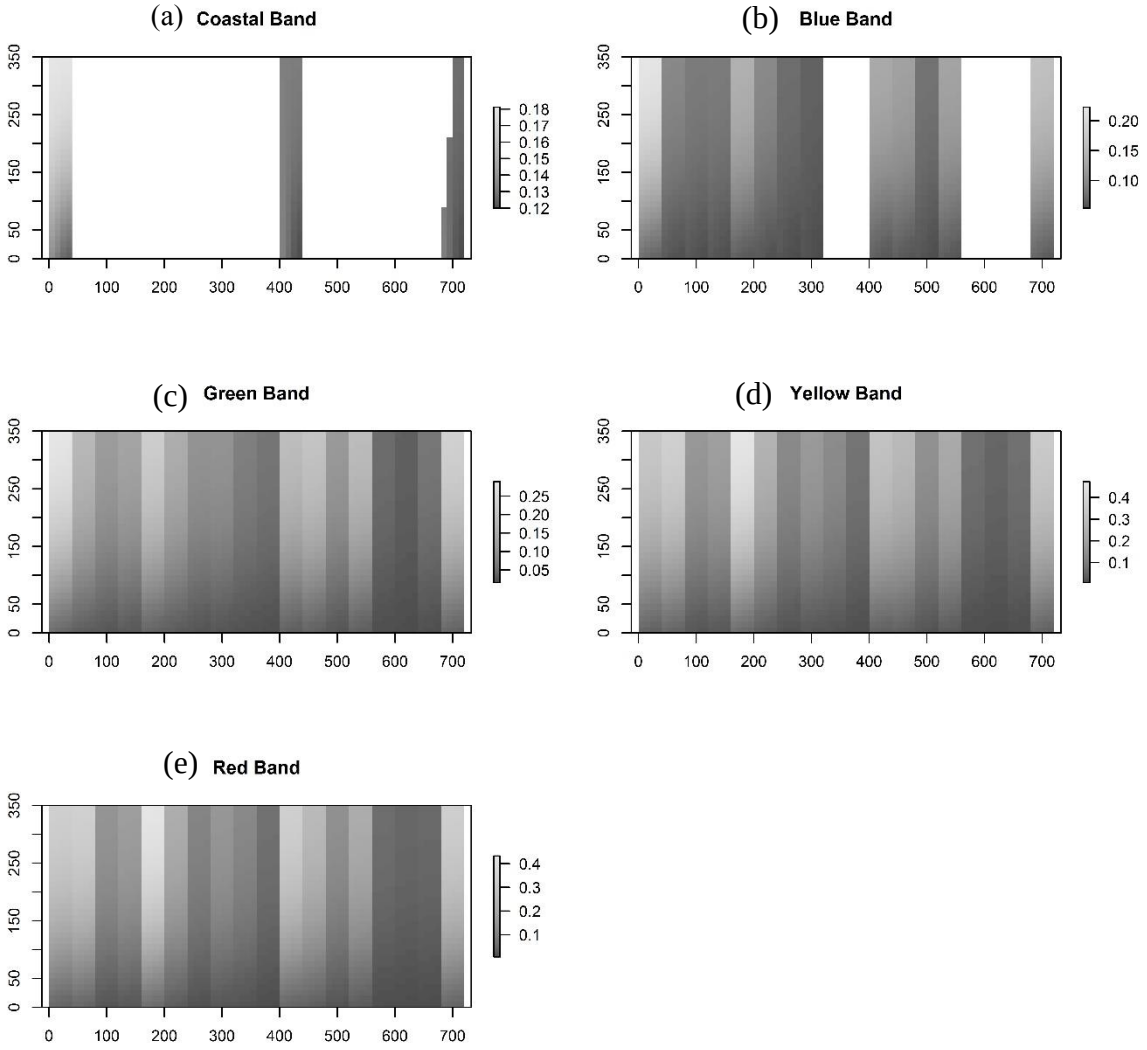

Figure 2. Simulated image of Maritonia et al.'s model:(a) Grey shaded of Coastal band, (b) Grey shaded of Blue band, (c) Grey shaded of Green band, (d) Grey shaded of Yellow band and (e) Grey shaded of Red band.

While the simulated image from Lee et al.'s model was shown in Figure 3. In the case of Lee et al.'s based simulated image, the two marked point from Maritonia et al.'s based simulated image was not applied. The dark object removal did not appear in any bands, and the coastal bands still give valuable information for all bottom types. Additionally, the attenuation effect of water depth was shown more intensively affected the just above surface reflectance especially in longer wavelength bands (Yellow and Red band).

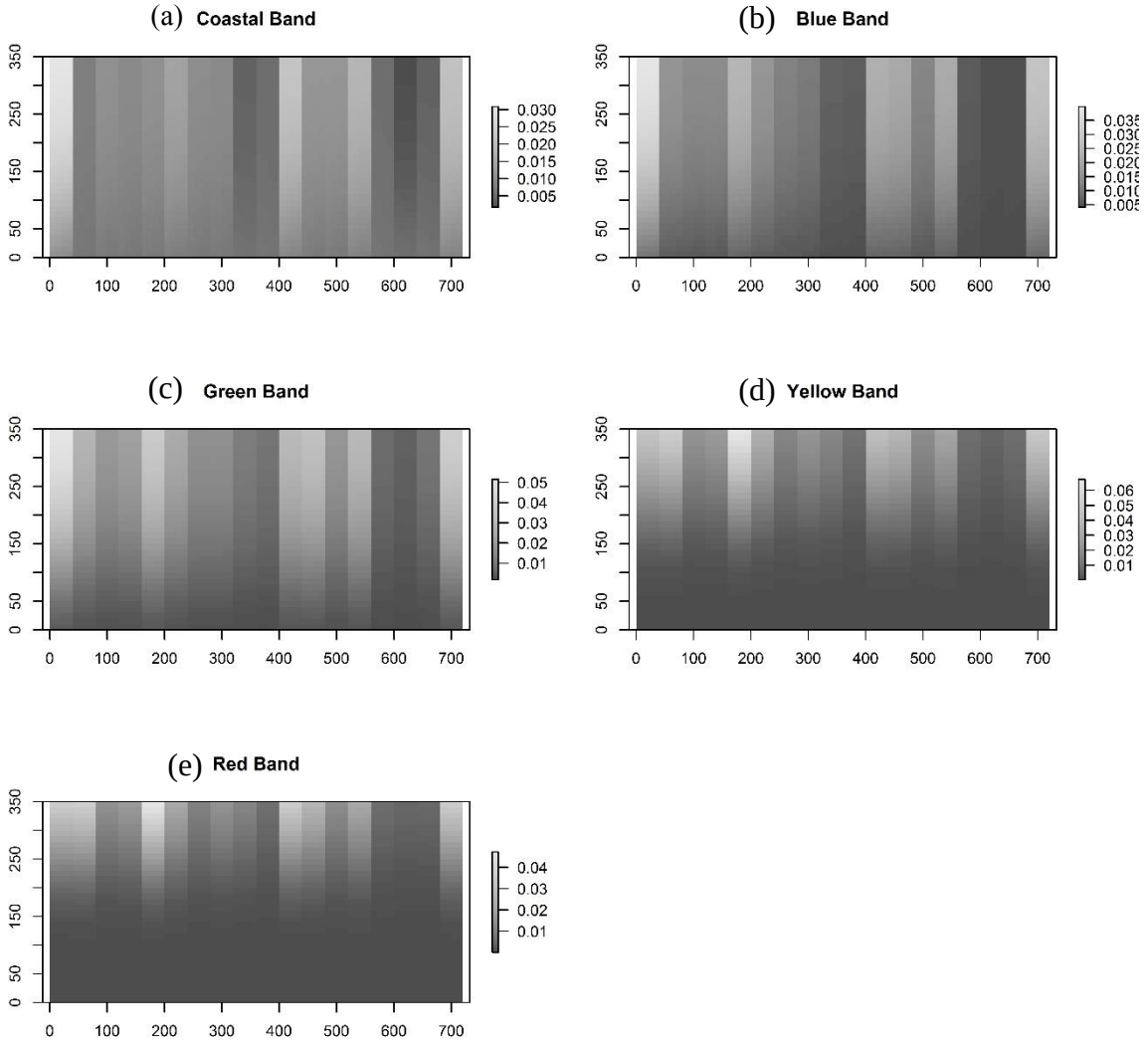

Figure 3. Simulated image of Lee et al.'s model:(a) Grey shaded of Coastal band, (b) Grey shaded of Blue band, (c) Grey shaded of Green band, (d) Grey shaded of Yellow band, and (e) Grey shaded of Red band

4. Performance of Lyzenga's Water Column Correction

The reflectance of visible bands (Figure 4.a. and 4.b) decreases follow with increasing depth, due to the exponential function of depth and attenuation coefficient (Equation 4 and 12). The effect of water attenuation for both models was different. In the case of Lee et al.'s model, the longer visible band wavelength (i.e., red band) shows a more dramatically effect of water attenuation. This result is consistent with Kirk [15], for wavelength higher than 550 nm the attenuation coefficient is increasing rapidly with depth, occur due to a high ratio of scattering and absorption.

Figure 4.b and 5.b shows the linearized reflectance (X_i) of Maritonia et al.'s and Lee et al.'s based simulated images, respectively. Theoretically, a straight line form is created if we plotted the linearized reflectance with depth, as the Maritonia et al.'s model performed (Figure 4.b). Since the Lee et al.'s based simulated images have more complex's relation between reflectance and depth the plotted linearized reflectance with a depth not show more curvy line form (Figure 5.b).

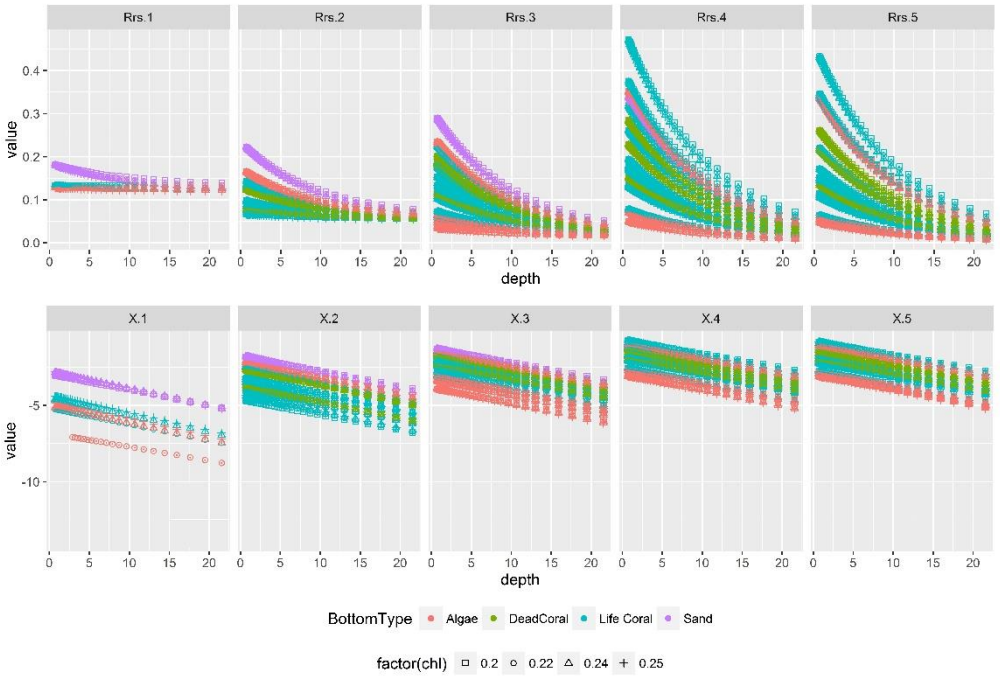

Figure 4. The scatterplot of each bottom type classes shows the effect of depth for Maritonia et al.'s model (a) reflectance value and depth, (b) linearized reflectance and depth

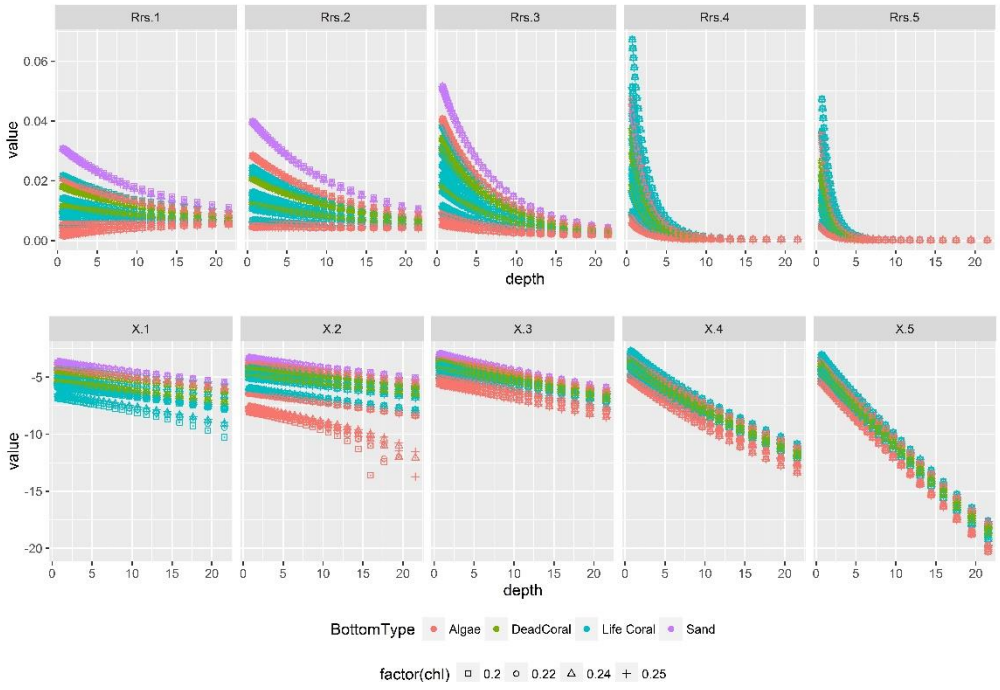

Figure 5. The scatterplot of each bottom type classes shows the effect of depth for Lee et al.'s model: (a) reflectance value and depth, (b) linearized reflectance and depth

4.1 The Removal of Water Attenuation Effect

The performance of Lyzenga's water column correction (Figure 6.a and 6.b) proved that the effect of scattering and absorption in the water column are reduced able. The performance of Lyzenga water column correction on Maritonia et al.'s based simulated images work as Lyzenga explains in the paper that depth invariance index is free of water attenuation effect, but the Lee et al.'s model result shows slightly different.

If the actual surface reflectance is more complicated thenMaritonia et al.'s reflectance model (Eq.4), as we used in the Lee et al.'s based simulated imagery. Then the Lyzenga water column correction could not remove the water attenuation effect but could reduce the effect. Another remaining problem in the case of Maritonia et al.'s model, where the slope ($\frac{k_i}{k_j}$) of each bottom types for some band pairs was sometimes not equal for each bottom types. This occurred due to the water quality variation. Even this study set the water quality in the range of 0.2 – 0.25 mg m-3 which in small difference. But the effect was significantly affecting an object with dark reflectances, such as algae.

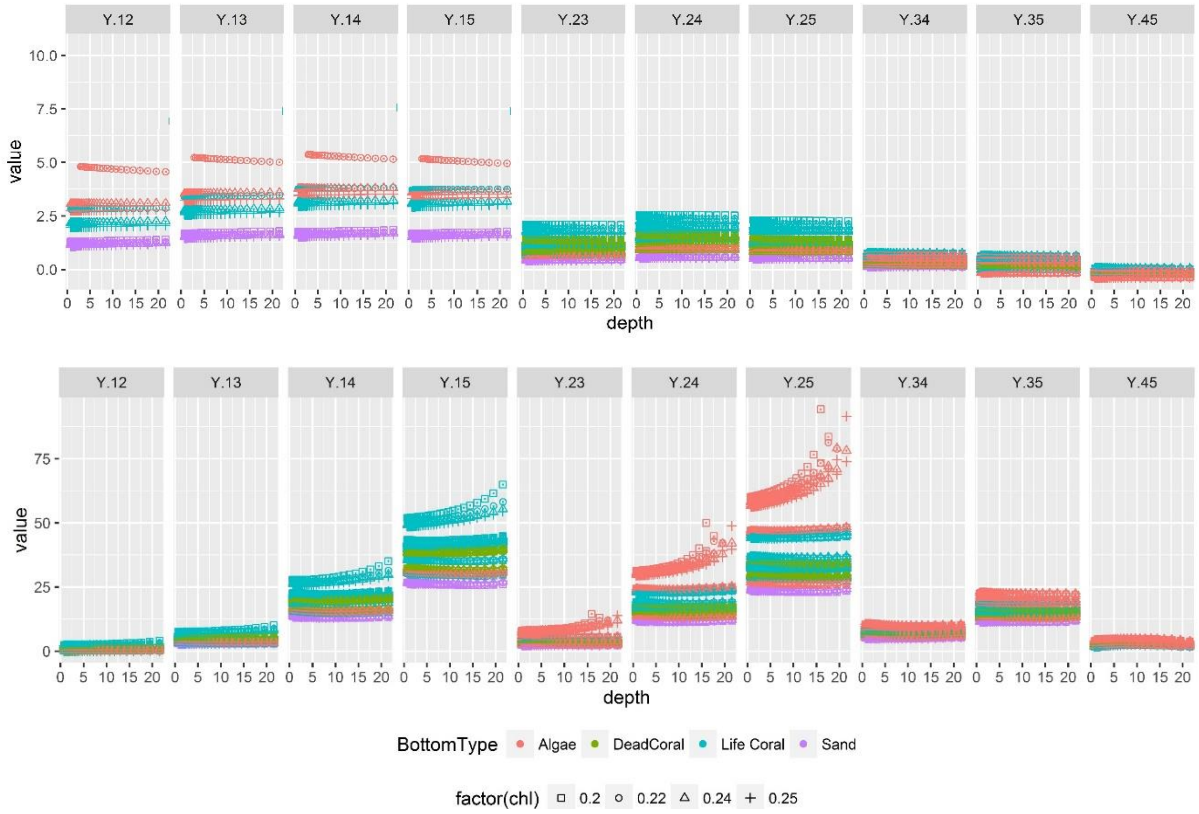

Figure 6. The depth invariance index for (a) Maritonia et al.'s and (b) Lee et al.'s model versus depth

5. Mathematical Explanation of Simulation Results

By using a mathematical expression, we check the performance of Lyzenga water column correction on simulated reflectance data. First for the Maritonia et al.'s model, the surface reflectance (Equation 13) that is an exponential function of depth are converted as a linear function of depth using Equation 1 and shows in detail as follows:

$$X_i = \log\left(\left(V_i + \left((p_{b_i} - V_i)e^{-hk_i}\right)\right) - \left(V_i + \left((p_{b_i} - V_i)e^{-\infty k_i}\right)\right)\right) \quad (21)$$

$$= \log\left(\left(V_i + \left((p_{b_i} - V_i)e^{-hk_i}\right)\right) - (V_i)\right)$$

$$= \log\left((p_{b_i} - V_i)e^{-hk_i}\right)$$

$$= \log(p_{b_i} - V_i) - hk_i$$

Then$m$ or the slope of two pair data for Maritonia et al.'s model is written as:

$$m = = \frac{\left(log(p_{b_i} - V_i) - hk_i\right)_{max} - \left(log(p_{b_i} - V_i) - hk_i\right)_{min}}{\left(log\left(p_{b_j} - V_j\right) - hk_j\right)_{max} - \left(log\left(p_{b_j} - V_j\right) - hk_j\right)_{min}} \quad (22)$$

To calculate m, Lyzenga's method assumed that the water quality is homogeneus and a single bottom type is used, then p_b, V and $k$value are the same all over depth range, thus the calculation of m simplyfied is as follows

$$m = \frac{k_i(h_{max} - h_{min})}{k_j(h_{max} - h_{min})} = \frac{k_i}{k_j} \quad (23)$$

Equation 23 shows that the slope of pair between two linearized reflectance of i and j bands is equal with $\frac{k_i}{k_j}$, then equation 3 could written as

$$Y_{ij} = \log(p_{b_i} - V_i) - hk_i - \frac{k_i}{k_j}\left(\log\left(p_{b_j} - V_j\right) - hk_j\right)$$

$$= \log(p_{b_i} - V_i) - \frac{k_i}{k_j}\log\left(p_{b_j} - V_j\right) \quad (24)$$

Then equation 24 shows that's no depth variable in the final product of Lyzenga's Water Column Correction.

Second for the Lee et al.'s model that shows water attenuation could not be removed. Then we evaluated the performance mathematically. Begin with substitute the Lee's surface reflectance function (Eq.2) to transformed reflectance equation (Eq.5) as follows

$$X_i = \log\left(\left(r_{rs\,i}^{dp}\left(1 - e^{-\left[\frac{1}{\cos(\theta_s)} + D_{u\,i}^{C}\right]k_i H}\right) + \frac{\rho_i}{\pi}e^{-\left[\frac{1}{\cos(\theta_s)} + D_{u\,i}^{B}\right]k_i H}\right) - \left(r_{rs\,i}^{dp}\right)\right)$$

$$= \log\left(\frac{\rho_i}{\pi}e^{-\left[\frac{1}{\cos(\theta_s)} + D_{u\,i}^{B}\right]k_i H} - r_{rs\,i}^{dp}e^{-\left[\frac{1}{\cos(\theta_s)} + D_{u\,i}^{C}\right]k_i H}\right) \quad (25)$$

In order to solve equation 2, $D_{u\,i}^{B} = 1.3786 D_{u\,i}^{C}$. Then the equation is simplified as

$$X_i = \log\left(\frac{\rho}{\pi}e^{-\left[\frac{1}{\cos(\theta_s)} + D_u^B\right]kH} - r_{rs}^{dp}e^{-\left[\frac{1}{\cos(\theta_s)} + D_u^C\right]kH}\right)$$

$$= \log\left(\frac{\rho}{\pi}e^{-\left[\frac{1}{\cos(\theta_s)} + 1.3786 D_u^C\right]kH} - r_{rs}^{dp}e^{-\left[\frac{1}{\cos(\theta_s)} + D_u^C\right]kH}\right)$$

$$= \log\left(\left(\frac{\rho}{\pi}e^{-\left[\frac{1}{\cos(\theta_s)} + 0.3786 D_u^C\right]kH} - r_{rs}^{dp}\right)e^{-\left[\frac{1}{\cos(\theta_s)} + D_u^C\right]kH}\right) \quad (26)$$

$$= -\left(\frac{1}{\cos(\theta_s)} + D_{u_i}^{C}\right)k_i H + \log\left(\frac{\rho_{b,i}}{\pi}e^{-\left[\frac{1}{\cos(\theta_s)} + 0.3786\mathrm{D}_{\mathrm{u}i}^{\mathrm{C}}\right]k_i H} - r_{rs\,i}^{dp}\right)$$

$$= -\left(\sec(\theta_s) + D_{u_i}^{C}\right)k_i H + \log\left(\frac{\rho_{b,i}}{\pi}e^{-\left[\sec(\theta_s) + 0.3786\mathrm{D}_{\mathrm{u}i}^{\mathrm{C}}\right]k_i H} - r_{rs\,i}^{dp}\right)$$

The transformed reflectance X_i for Lee's reflectance is shown in Equation 26. Then the slope of pair X_i and $X_j$for Lee et al.'s model was follow

$$m = \frac{\left(-\left(\sec(\theta_s) + D_{u_i}^C\right)k_i H + log\left(\frac{\rho_{b,i}}{\pi} e^{-\left[\sec(\theta_s) + 0.3786 D_{u_i}^C\right]k_i H} - r_{rs\ i}^{dp}\right)\right)_{max} - \left(-\left(\sec(\theta_s) + D_{u_i}^C\right)k_i H + \log\left(\frac{\rho_{b,i}}{\pi} e^{-\left[\sec(\theta_s) + 0.3786 D_{u_i}^C\right]k_i H} - r_{rs\ i}^{dp}\right)\right)_{min}}{\left(-\left(\sec(\theta_s) + D_{u_j}^C\right)k_j H + log\left(\frac{\rho_{b,j}}{\pi} e^{-\left[\sec(\theta_s) + 0.3786 D_{u_j}^C\right]k_j H} - r_{rs\ j}^{dp}\right)\right)_{max} - \left(-\left(\sec(\theta_s) + D_{u_j}^C\right)k_j H + log\left(\frac{\rho_{b,j}}{\pi} e^{-\left[\sec(\theta_s) + 0.3786 D_{u_j}^C\right]k_j H} - r_{rs\ j}^{dp}\right)\right)_{min}} \quad (27)$$

As explain in subchapter 2.2, Lyzenga's method assumed that the water quality is homogeneus and a single bottom type is used, then p_b, V and $k$value are the same all over depth range, thus the calculation of m is written as follows

$$\begin{aligned} m &= \frac{-\left(\sec(\theta_s) + D_{u_i}^C\right)k_i H_{max} + \left(\sec(\theta_s) + D_{u_i}^C\right)k_i H_{min} + \log\left(\frac{\rho_{b,i}}{\pi} e^{-\left[\sec(\theta_s) + 0.3786 D_{u_i}^C\right]k_i H_{max}} - r_{rs\ i}^{dp}\right) - \log\left(\frac{\rho_{b,i}}{\pi} e^{-\left[\sec(\theta_s) + \right.}\right.}{-\left(\sec(\theta_s) + D_{u_i}^C\right)k_i H_{max} + \left(\sec(\theta_s) + D_{u_i}^C\right)k_i H_{min} + \log\left(\frac{\rho_{b,i}}{\pi} e^{-\left[\sec(\theta_s) + 0.3786 D_{u_i}^C\right]k_i H_{max}} - r_{rs\ i}^{dp}\right) - \log\left(\frac{\rho_{b,i}}{\pi} e^{-\left[\sec(\theta_s) + \right.}\right.} \\ &= \frac{\left(\sec(\theta_s) + D_{u_i}^C\right)k_i (H_{min} - H_{max}) + \log\left(\frac{\frac{\rho_{b,i}}{\pi} e^{-\left[\sec(\theta_S) + 0.3786 D_{u_i}^C\right]k_i H_{max}} - r_{rs\ i}^{dp}}{\frac{\rho_{b,i}}{\pi} e^{-\left[\sec(\theta_S) + 0.3786 D_{u_i}^C\right]k_i H_{min}} - r_{rs\ i}^{dp}}\right)}{\left(\sec(\theta_s) + D_{u_j}^C\right)k_j (H_{min} - H_{max}) + \log\left(\frac{\frac{\rho_{b,j}}{\pi} e^{-\left[\sec(\theta_S) + 0.3786 D_{u_j}^C\right]k_j H_{max}} - r_{rs\ j}^{dp}}{\frac{\rho_{b,j}}{\pi} e^{-\left[\sec(\theta_S) + 0.3786 D_{u_j}^C\right]k_j H_{min}} - r_{rs\ j}^{dp}}\right)} \\ &= \frac{\left(\sec(\theta_s) + D_{u_i}^C\right)_{k_i}}{\left(\sec(\theta_s) + D_{u_j}^C\right)_{k_j}} \end{aligned} \quad (28)$$

Assumed that $\log\left(\frac{\frac{\rho_{b,i}}{\pi} e^{-\left[\sec(\theta_S) + 0.3786 D_{u_i}^C\right]k_i H_{max}} - r_{rs\ i}^{dp}}{\frac{\rho_{b,i}}{\pi} e^{-\left[\sec(\theta_S) + 0.3786 D_{u_i}^C\right]k_i H_{min}} - r_{rs\ i}^{dp}}\right)$ and $\log\left(\frac{\frac{\rho_{b,j}}{\pi} e^{-\left[\sec(\theta_S) + 0.3786 D_{u_j}^C\right]k_j H_{max}} - r_{rs\ j}^{dp}}{\frac{\rho_{b,j}}{\pi} e^{-\left[\sec(\theta_S) + 0.3786 D_{u_j}^C\right]k_j H_{min}} - r_{rs\ j}^{dp}}\right)$will give a very small value than could be neglected then Equation 28 shows that the slope of a pair between band i and j in the case of Lee et al.'s model was not only the attenuation coefficient ratio but include the and solar zenith value. Finally, the Depth Invariance Index equation (Eq. 3) for Lee's model can be simplified and expressed as

$$\begin{aligned} Y_{ij} &= \left(-\left(\sec(\theta_s) + D_{u_i}^C\right)k_i H + \log\left(\frac{\rho_{b,i}}{\pi} e^{-\left[\sec(\theta_s) + 0.3786 D_{u_i}^C\right]k_i H} - r_{rs}\right)\right) \\ &- \frac{\left(\sec(\theta_s) + D_{u_i}^C\right)_{k_i}}{\left(\sec(\theta_s) + D_{u_j}^C\right)_{k_j}}\left(-\left(\sec(\theta_s) + D_{u_j}^C\right)k_j H + \log\left(\frac{\rho_{b,j}}{\pi} e^{-\left[\sec(\theta_s) + 0.3786 D_{u_j}^C\right]k_j H} - r_{rs}\right)\right) \end{aligned} \quad (29)$$

$$= \log\left(\frac{\rho_{b,i}}{\pi} e^{-0.378633 D_{u_i}^C k_i H} - r_{rs\ i}^{dp}\right) - \log\left(\frac{\rho_{b,j}}{\pi} e^{-0.378633 D_{u_j}^C k_j H} - r_{rs\ j}^{dp}\right)\left(\frac{\left(\sec(\theta_s) + D_{u_i}^C\right)_{k_i}}{\left(\sec(\theta_s) + D_{u_j}^C\right)_{k_j}}\right)$$

Above equation shows the Lyzenga water column method could not remove the effect of depth and water attenuation. In fact, the effect of depth and water attenuation are in multiplication function. Thus, even after the correction, the water column attenuation effect will remain. In the case of IOP with chlorophyll-a between 0.2 – 0.25 mg m-3, if the attenuation coefficient is small such us blue band (kblue ≈ 0.04) or green band (kgreen ≈ 0.06) then the depth invariance index have less water column effect. More over, a failure of correction will occur for the pair of a longer visible band wavelength,

namely red band, due to the high attenuation coefficient (kred ≈ 0.4) that reach 9 and 6 times more higher than in the blue and green band, respectively.

One downside regarding this study is that each bottom type had been set to have the same opportunity to appear in the same number and same depth, which unnaturally thing happen in the coral reef ecosystem. Unfortunately, there is no scientific information about the representative distribution of each bottom types. It became the limitation to made more natural simulated imagery with representative distribution in the coral reef environment. However, the initial simulated imagery already answers the main aim of identifying the performance of Lyzenga's water column correction.

6. Conclusion

The simulated imagery provides powerful tools for imagery or methodology evaluation. Our investigation on simulated Worldview-2 imagery over coral reef environment shows that the Lyzenga's water column correction plays differently in both Maritonia et al.'s and Lee et al.'s surface reflectance model. In the case of Maritonia et al.'s based simulated image, the effect of attenuation coefficient was almost removable in any pair of six visible bands. While, for the Lee et al.'s based simulated image the Lyzenga water column correction tecnique was only able to reduce the effect of water attenuation. Supprisingly, the assumption that ratio of attenuation coefficient is equal at any bottom types was hardly to proven. In our simulation, a slight variation in water quality (0.2 - 0.25 mg m-3) variation shows an significant effect on the performance of Lyzenga's water column correction.

The present study has only examined the effect of water column correction under zero noise condition, which gave a positive result. Therefore, the other factor that is influencing the just aboved surface reflectance should be investigated, such as noise, bottom types diversity, intermixing pixels, water quality, and number of representative sample. Research into solving several of this problems is already underway.

7. Acknowledgement

The first author acknowledges support from the Indonesia Endowment Fund for Education (LPDP) by the Ministry of Finance. We are very grateful to Marlina Nurlidiasariforgave permission to use her spectral measurement data.

References

[1] Lyzenga, D.R 1978 Passive remote sensing techniques for mapping water depth and bottom features *Applied Optic***17**(3) pp 379–383.

[2] Pulliza, DT 2004 A Multi-Sensor Comparison For Coral Reef Habitat Mapping: A Case Study Using A Tropical Patch Reef Environment In Biscayne National Park, Florida (Doctoral Dissertation, University OF Puerto Rico Mayaguez Campus).

[3] Pahlevan, N.; Valadanzouj, M.; Alimohamadi A 2006 A Quantitative Comparison to Water Column Correction Reference 1Techniques for Benthic Mapping Using High Spatial Resolution Data. Paper presented at the ISPRS Commission VII Mid-term Symposium *Remote Sensing, From Pixels to Processes*(Enschede, The Netherlands)

[4] Nurlidiasari, M., Budiman, S 2005 Mapping coral reef habitat with and without water column correction using Quickbird image *International Journal of Remote Sensing and Earth Science***2**pp 45–56.

[5] Sagawa, T., Mikami, A., Aoki, M.N., and Komatsu, T 2012 Mapping seaweed forests with IKONOS image based on bottom surface reflectance *Proc. SPIE* **8525**: 85250Q. doi: 10.1117/12.975678

[6] Budhiman, S., Parwati, E., and Emiyati 2012 The effect of the extent of coral reef area on uniform bottom reflectance determination for water column correction using Landsat ETM *International Journal of Remote Sensing and Earth Sciences (IJReSES)* **9**(2) pp 88-99.

[7] Purkis, SJ and Pasterkamp, R 2004 Integrating in situ reef-top reflectance spectra with Landsat TM imagery to aid shallow-tropical benthic habitat mapping *Coral reef*. **23**(1) pp 5-20

[8] Mishra, D.R., Narumalani, S., Rundquist, D., Lawson M 2005 High-resolution ocean color remote sensing of benthic habitats: a case study at the Roatan Island, Honduras *IEEE Geoscience and Remote Sensing Letters***43**(7) pp 1592--1604
[9] Zoffoli, M. L., Frouin, R., and Kampel M 2014 Water column correction for coral reef studies by remote sensing *Sensors***14**(9), 16881-16931.
[10] Gordon, HR, Brown, OB, and Ando Jacobs, MM 1975 Computed Relationships Between The Inherent And Apparent Optical Properties Of A Flat Homogeneous Ocean *Applied Optics***14** (2), pp 417-427.
[11] Maritorena, S., Morel, A., and Gentili, B 1994 Diffuse reflectance of oceanic shallow waters: Influence of water depth and bottom albedo *Limnology and oceanography***39**(7), pp 1689-1703.
[12] Lafon, V., Froidefond, J. M., Lahet, F., and Castaing P 2002 SPOT shallow water bathymetry of a moderately turbid tidal inlet based on field measurements *Remote sensing of Environment***81**(1), pp 136-148.
[13] Lee, Z.P., and K.L. Carder 1999 Effect of spectral band numbers on the retrieval of water column and bottom properties from ocean color data *Applied Optic***41**(12) pp 2191-2201.
[14] Lee, Z.P., A. Weidemann, and R. Arnone 2013 Combined effect of reduced band number and increased bandwidth on shallow water remote sensing: the case of Worldview-2 *IEEE Trans. Geoscience and Remote Sensing***51** (5) pp 2577-2586.
[15] Kirk, J.T.O 1981Estimation of the scattering coefficient of natural waters using underwater irradiance measurements *Australia Journal of marine Freshwater Research***32** pp 533-539.